Article

Cell Reports

Activin E Controls Energy Homeostasis in Both Brown and White Adipose Tissues as a Hepatokine

Graphical Abstract

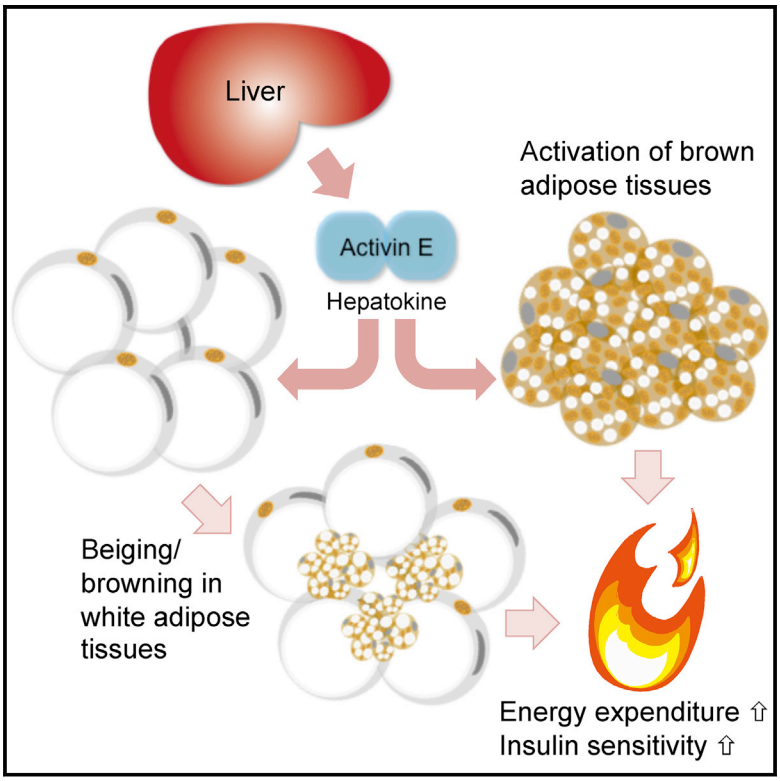

Authors

Osamu Hashimoto, Masayuki Funaba, Kazunari Sekiyama, ..., Seiichi Oyadomari, Hiromu Sugino, Akira Kurisaki

Correspondence

ohashim@vmas.kitasato-u.ac.jp (O.H.), mfunaba@kais.kyoto-u.ac.jp (M.F.), akikuri@bs.naist.jp (A.K.)

In Brief

Hashimoto et al. show that activin E, a member of the transforming growth factor-β superfamily, functions as a hepatokine. Activin E stimulates energy expenditure and increases insulin sensitivity through brown and beige adipocyte activation, suggesting a possible preventive or therapeutic target for obesity.

Highlights

- Hepatic overexpression of activin E (Alb-ActE) activates thermogenesis
- Alb-ActE induces emergence of beige adipocytes and improved insulin sensitivity
- Knockout of activin E gene inhibits cold-induced Ucp1 in inguinal fat depot
- Activin E directly stimulates expression of Ucp1 in cultured brown adipocytes

Hashimoto et al., 2018, Cell Reports *25*, 1193–1203
October 30, 2018
https://doi.org/10.1016/j.celrep.2018.10.008

CellPress

Cell Reports
Article

Activin E Controls Energy Homeostasis in Both Brown and White Adipose Tissues as a Hepatokine

Osamu Hashimoto,[1,8,*] Masayuki Funaba,[2,*] Kazunari Sekiyama,[1] Satoru Doi,[1] Daichi Shindo,[1] Ryo Satoh,[1] Hiroshi Itoi,[1] Hiroaki Oiwa,[1] Masahiro Morita,[1] Chisato Suzuki,[1] Makoto Sugiyama,[1] Norio Yamakawa,[3] Hitomi Takada,[3,4] Shigenobu Matsumura,[5] Kazuo Inoue,[5] Seiichi Oyadomari,[6] Hiromu Sugino,[3,7] and Akira Kurisaki[3,4,*]

[1]Faculty of Veterinary Medicine, Kitasato University School of Veterinary Medicine, Towada, Aomori 034-8628, Japan
[2]Division of Applied Biosciences, Graduate School of Agriculture, Kyoto University, Kitashirakawa Oiwakecho, Kyoto 606-8502, Japan
[3]Research Center for Stem Cell Engineering, National Institute of Advanced Industrial Science and Technology (AIST), Tsukuba, Ibaraki 305-8562, Japan
[4]Division of Biomedical Sciences, Stem Cell Technology Laboratory, Graduate School of Biological Sciences, Nara Institute of Science and Technology (NAIST), 8916-5 Takayama-cho, Ikoma 630-0192, Japan
[5]Division of Food Science and Biotechnology, Graduate School of Agriculture, Kyoto University, Kitashirakawa Oiwakecho, Kyoto 606-8502, Japan
[6]Division of Molecular Biology, Institute for Genome Research, The University of Tokushima, 3-18-15 Kuramoto, Tokushima 770-8503, Japan
[7]Present address: Tokyo Metropolitan Institute of Medical Science, 2-1-6 Kamikitazawa Setagaya, Tokyo 156-8506, Japan
[8]Lead Contact
*Correspondence: ohashim@vmas.kitasato-u.ac.jp (O.H.), mfunaba@kais.kyoto-u.ac.jp (M.F.), akikuri@bs.naist.jp (A.K.)
https://doi.org/10.1016/j.celrep.2018.10.008

SUMMARY

Brown adipocyte activation or beige adipocyte emergence in white adipose tissue (WAT) increases energy expenditure, leading to a reduction in body fat mass and improved glucose metabolism. We found that activin E functions as a hepatokine that enhances thermogenesis in response to cold exposure through beige adipocyte emergence in inguinal WAT (ingWAT). Hepatic activin E overexpression activated thermogenesis through Ucp1 upregulation in ingWAT and other adipose tissues including interscapular brown adipose tissue and mesenteric WAT. Hepatic activin E-transgenic mice exhibited improved insulin sensitivity. Inhibin βE gene silencing inhibited cold-induced Ucp1 induction in ingWAT. Furthermore, *in vitro* experiments suggested that activin E directly stimulated expression of *Ucp1* and *Fgf21*, which was mediated by transforming growth factor-β or activin type I receptors. We uncovered a function of activin E to stimulate energy expenditure through brown and beige adipocyte activation, suggesting a possible preventive or therapeutic target for obesity.

INTRODUCTION

Adipose tissue plays a vital role in regulation of whole-body energy metabolism. White adipose tissue (WAT) functions as an energy storage depot, whereas brown adipose tissue (BAT) is an energy dissipation depot. White adipocytes have a unilocular lipid droplet, and brown adipocytes are characterized by multilocular lipid droplets, densely packed mitochondria, and unique expression of uncoupling protein 1 (Ucp1). Ucp1 enables energy to dissipate as heat by uncoupling oxidative phosphorylation with ATP production (Cannon and Nedergaard, 2004). In addition to classical brown adipocytes (Seale et al., 2008; Lepper and Fan 2010), distinct Ucp1-positive adipocytes, so-called beige adipocytes, can be induced sporadically within WAT upon cold exposure (Vitali et al., 2012).

Adaptations to the cold are predominantly controlled by sympathetic nerves. Norepinephrine secreted by sympathetic nerves activates brown and beige adipocytes via β-adrenergic receptors, resulting in acceleration of lipolysis and upregulation of Ucp1 expression (Cousin et al., 1992; Wu et al., 2012). Although activation of brown and beige adipocytes may be a promising strategy against obesity, pharmacological activation of the sympathetic nervous system is not considered as a potential therapy because of strong side effects on the cardiovascular system (Yen and Ewald, 2012). Thus, identification of non-sympathetic regulators of brown and beige adipocyte activity has attracted great interest (Cereijo et al., 2015). Several factors, such as Fgf21, Bmp8b, and Irisin, have been shown to regulate brown and beige adipogenesis and activation of brown and beige adipocytes (Harms and Seale 2013).

Activin E, a secreted peptide encoded by the inhibin βE gene (*Inhbe*), is a member of the transforming growth factor-β (TGF-β) superfamily, which is predominantly expressed in the liver (Fang et al., 1997; Hashimoto et al., 2002). Activin E has been reported to inhibit proliferation of hepatocytes *in vitro* (Vejda et al., 2003; Wada et al., 2005) and *in vivo* (Chabicovsky et al., 2003). However, the effect is relatively small, and the physiological role of activin E has not been well defined (Lau et al., 2000). Here, we demonstrate that activin E is a peptide that activates the thermogenic program in adipose tissues and improves insulin sensitivity. We show that transgenic mice expressing

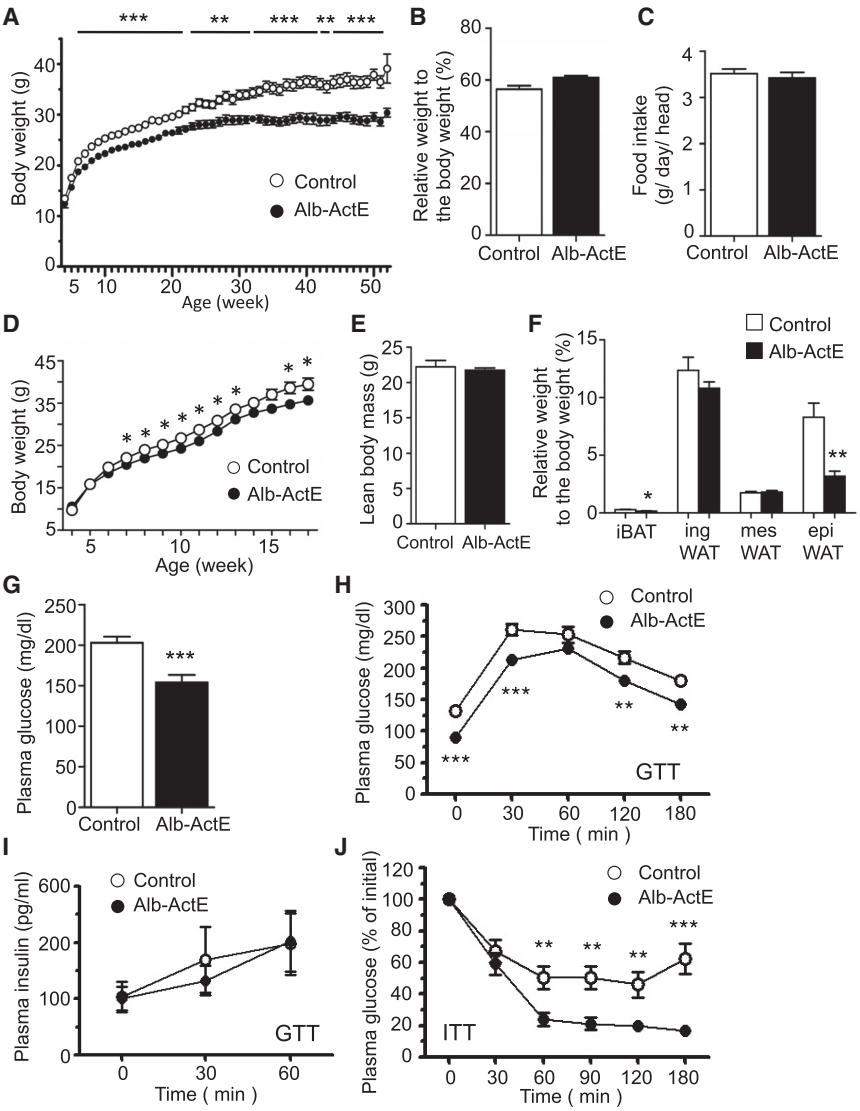

Figure 1. Body Weight and Glucose Metabolism of Liver-Specific Activin E-Overexpressing Mice

(A) Growth curve of Alb-ActE mice fed the control diet. Body weights of control and Alb-ActE mice were measured weekly from week 4 to 52. Values are the mean ± SEM. n = 11–14 in each group.

(B) Relative percentage of lean body weight to body weight of male Alb-ActE mice at 18–24 weeks of age fed the control diet. n = 6 in each group.

(C) Food intake of Alb-ActE mice at 16–21 weeks of age. n = 9–14 in each group.

(D) Growth curve of male Alb-ActE mice fed the high-fat diet. Body weights of control and Alb-ActE mice were measured weekly from week 4 to 17. Values are the mean ± SEM. n = 6 in each group.

(E) Lean body weight of Alb-ActE mice at 18 weeks of age fed the high-fat diet. n = 6 in each group.

(F) Adipose tissue weight in Alb-ActE mice. Relative tissue weight is expressed as the percentage of total body weight. Results are shown as means ± SEM. *p < 0.05 and **p < 0.01. n = 6 in each group.

(G) Blood glucose levels of mice (11–12 weeks old) fasted for 4 hr. n = 11 or 12.

(H and I) Glucose tolerance tests in Alb-ActE mice at 10–11 weeks of age. Blood glucose (H) and insulin (I) concentrations were measured at the indicated times. n = 9 or 10 in each group.

(J) Insulin tolerance tests in Alb-ActE mice at 11–12 weeks of age. Alb-ActE mice, liver-specific activin E-overexpressing mice. n = 9 or 10 in each group. Values are the mean ± SEM. *p < 0.05, **p < 0.01, and ***p < 0.001.

activin E in their liver exhibit induced emergence of beige adipocytes and activated brown adipocytes. As a result, thermogenesis is stimulated, leading to improvement of insulin sensitivity. Consistent with these results, targeted disruption of the inhibin or activin βE gene inhibited cold-induced thermogenesis and diet-induced obesity. We propose that activin E is a potential candidate for prevention or therapeutic intervention of obesity.

RESULTS

Improvement of Insulin Sensitivity in Transgenic Mice Overexpressing Hepatic Activin E

Previous reports have described fluctuation of activin E (*Inhbe*) mRNA expression in the rodent liver according to the nutritional status such as fasting, feeding, or chronic high calorie intake (Rodgarkia-Dara et al., 2006; Hashimoto et al., 2009). We confirmed the enhanced hepatic *Inhbe* mRNA level in mice fed a high-fat diet for 2 weeks (Figure S1A). In addition, *Inhbe* mRNA was predominantly expressed in the liver (Figure S1B). These findings prompted us to form the hypothesis that activin E may also function as a hormone that regulates energy homeostasis.

To examine the involvement of activin E in regulation of metabolic pathways, we generated transgenic mice overexpressing activin E in their liver under the control of the albumin promoter (Alb-ActE mice; Figures S2A–S2F). Compared with control mice, body weight gain was less in Alb-ActE mice (Figure 1A). The reduction of body weight gain did not result from a decrease in lean body mass (Figure 1B). In addition, daily food intake was not affected in Alb-ActE mice (Figure 1C). When mice were fed the high-fat diet, Alb-ActE mice exhibited partial resistance to diet-induced obesity (Figure 1D) without affecting their lean body mass (Figure 1E). Moreover, the epididymal WAT (epiWAT) weight was significantly decreased in Alb-ActE mice fed the high-fat diet (Figure 1F).

We next evaluated glucose metabolism in Alb-ActE mice. Alb-ActE mice showed a marked decrease in their plasma glucose level compared with control mice (Figure 1G). A glucose tolerance test indicated that the plasma glucose level was significantly lower in Alb-ActE mice compared with the control group

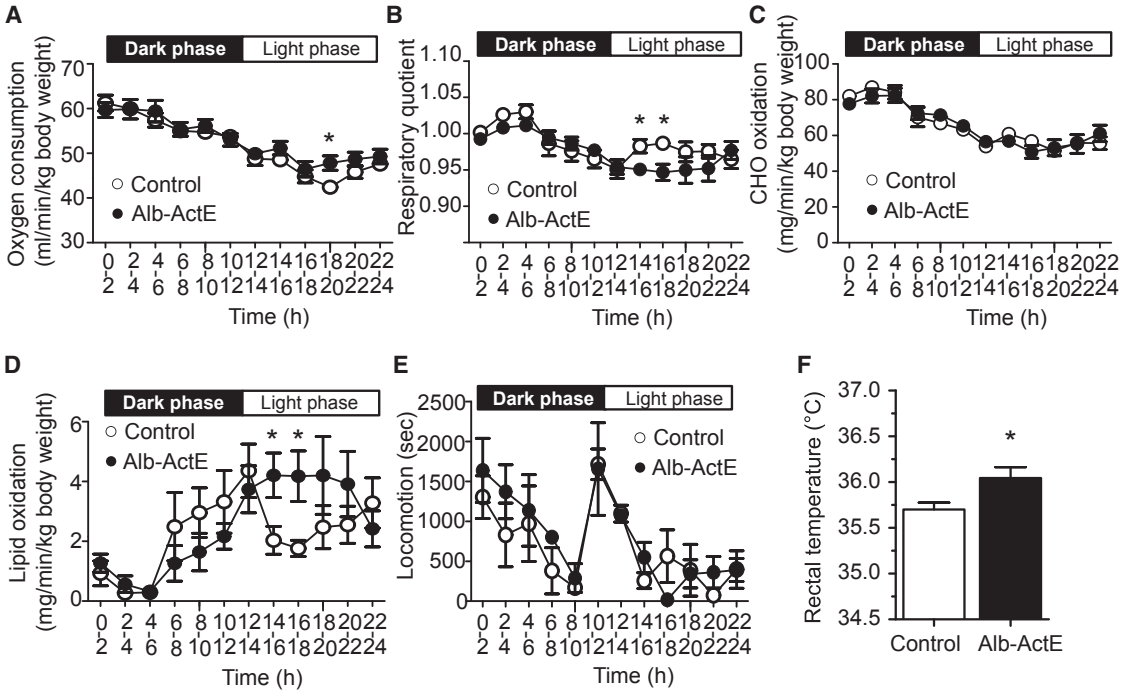

Figure 2. Energy Metabolism of Alb-ActE Mice

(A–D) Oxygen consumption (A), respiratory exchange ratio (B), carbohydrate oxidation (C), and lipid oxidation (D) of Alb-ActE mice at 9–11 weeks of age (n = 8). Data on oxygen consumption and oxidation of carbohydrate and lipid are shown as milliliters per minute per kilogram of total body weight.

(E and F) Locomotion of 14-week-old Alb-ActE mice (n = 4) (E) and rectal temperature of Alb-ActE mice at 29–34 weeks of age measured during the light phase (n = 9–14) (F). CHO, carbohydrates. Values are means ± SEM. *p < 0.05.

before and after glucose challenge (Figure 1H). Estimation of the area under curve was also lower in Alb-ActE mice (control mice, 8.88 ± 0.32; Alb-ActE mice, 7.30 ± 0.17; $p < 0.001$). Plasma insulin levels were comparable between the groups, suggesting that the decrease in the plasma glucose level was not due to an increase of insulin secretion (Figure 1I). An insulin tolerance test indicated that the decrease in the plasma glucose level was more remarkable in Alb-ActE mice than in control mice after insulin challenge (Figure 1J), suggesting that activin E has a function to enhance insulin sensitivity. Overexpression of hepatic activin E did not affect serum levels of triglycerides, aspartate aminotransferase (AST), and alanine aminotransferase (ALT), or the relative weights of organs such as the liver, pancreas, kidney, heart, and testis (Figures S2G–S2J). In addition, histological analysis indicated that Alb-ActE mice did not exhibit any pathological abnormalities (Figure S3).

Activation of Fat Metabolism by Overexpression of Hepatic Activin E

To investigate the metabolic consequences of activin E overexpression, we subjected Alb-ActE mice to indirect calorimetry. Simultaneous measurements of oxygen consumption and carbon dioxide production allow determination of the respiratory quotient (RQ) that reflects the carbohydrate and fat oxidation ratio unless protein metabolism is altered substantially. The volume of oxygen consumed by Alb-ActE mice was higher than that by control mice during the light phase (Figure 2A). In contrast, the RQ during the light phase was lower in Alb-ActE mice than in control mice (Figure 2B). These measurements revealed that the amount of oxidized carbohydrate was not different between these mice. However, lipid oxidation was enhanced in Alb-ActE mice during the light phase compared with control mice (Figures 2C and 2D). Differential body weight was not responsible for the results; analysis of covariance (ANCOVA) analysis (Tschöp et al., 2011) with genotype and body weight as factors of raw data indicated similar tendency on genotype effect (Figures S2K–S2N). We found no marked differences in locomotive activity between these mice (Figure 2E). The results suggested that the improved insulin sensitivity in Alb-ActE mice was related to increased energy expenditure during sleep, particularly by activation of lipid oxidation. Furthermore, the rectal temperature was higher in Alb-ActE mice compared with control mice (Figure 2F).

Activation of Brown Adipocytes and Emergence of Beige Adipocytes in Alb-ActE Mice

The above results raised the possibility that the increase in energy expenditure was due to enhanced heat production by brown adipocytes, beige adipocytes, or both. Thus, we characterized adipose tissues in Alb-ActE mice. The relative weight of interscapular BAT (iBAT) was decreased (Figure 3A), and the brown adipocyte size was slightly increased compared with control mice (Figures 3B and 3C). Immunoblot analysis indicated

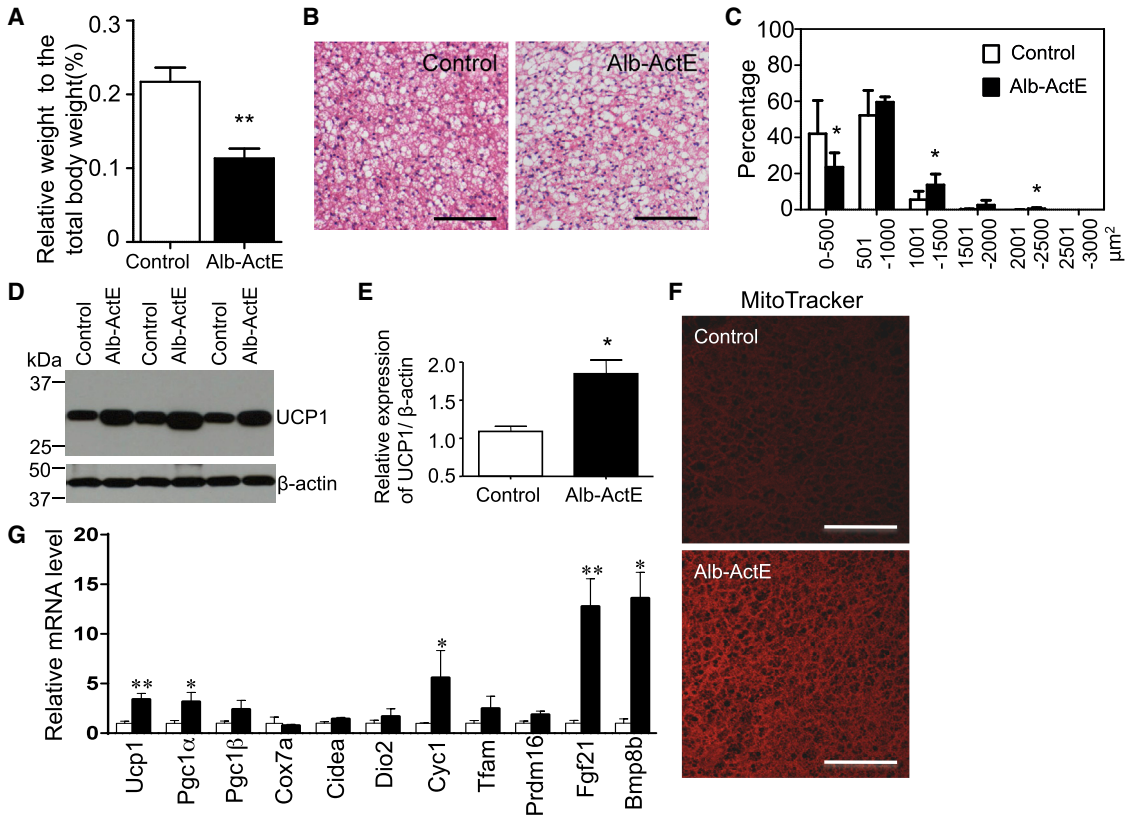

Figure 3. Characteristics of iBAT in Alb-ActE Mice

(A) iBAT weight in Alb-ActE mice. Relative tissue weight is expressed as a percentage of total body weight. Results are shown as means ± SEM. *$p < 0.05$. n = 4 in each group (18–24 weeks of age).

(B) Histological analysis of iBAT in Alb-ActE mice (18 weeks of age). Adipose tissue sections were stained with H&E. Representative data are shown. Bar, 100 μm.

(C) Distribution of the cell size in iBAT of Alb-ActE mice. Tissue sections were stained with H&E. The adipocyte size in arbitrary fields of view was analyzed by ImageJ. Results are shown as means ± SEM. *$p < 0.05$. n = 4 in each group (18–24 weeks of age).

(D) Western blot analysis of UCP1 expression in iBAT of Alb-ActE mice (12 weeks of age). iBAT was lysed with RIPA buffer and subjected to western blotting. Representative data are shown.

(E) Densitometric values for UCP1 expression in E. Data represent means ± SEM. *$p < 0.05$. n = 4 in each group.

(F) Fluorescence staining of mitochondria in iBAT from Alb-ActE mice (18 weeks of age). iBAT sections were reacted with MitoTracker. Fluorescent signals were observed using a fluorescence microscope. Representative data are shown. Bar, 100 μm.

(G) Gene expression of brown adipocyte-specific genes in iBAT of Alb-ActE mice. iBAT mRNA from the mice was subjected to RT-qPCR. Expression of the genes was normalized to that of Hprt1. The expression level in control mice was set at 1. Data are shown as the mean ± SEM. *$p < 0.05$ and **$p < 0.01$. n = 4 in each group (24–27 weeks of age).

stronger expression of Ucp1 in iBAT of Alb-ActE mice than in that of control mice (Figures 3D and 3E). Staining of brown adipocytes with MitoTracker, a mitochondrion-specific dye, revealed an increase in the number of mitochondria (Figure 3F). In addition, expression of genes related to brown and beige adipocytes was generally increased in iBAT of Alb-ActE mice compared with that of control mice (Figure 3F). In particular, expression of *Fgf21* and *Bmp8b* was significantly higher in Alb-ActE mice than in control mice (Figure 3G). These molecules stimulate activation of brown and beige adipocytes (Fisher et al., 2012; Whittle et al., 2012).

We also characterized WAT of Alb-ActE mice. Overexpression of hepatic activin E decreased the relative weight of WAT compared with control mice (Figure 4A). The weight of mesenteric WAT (mesWAT) was also significantly lower. Histological analysis revealed an increase in the occurrence of multiple lipid droplets and acidophilic adipocytes, especially in inguinal WAT (ingWAT) and mesWAT, but not in epiWAT (Figures 4B–4D). A significant reduction of the adipocyte size was also apparent in ingWAT and mesWAT, while the percentage of large adipocytes (>8,000 μm^2) was higher in epiWAT of Alb-ActE mice (Figure S4). Immunohistochemical analysis showed induction of Ucp1-positive multilocular adipocytes among white adipocytes in ingWAT and mesWAT of Alb-ActE mice (Figures 4E and 4F). The mitochondrial density was also increased in these WATs of Alb-ActE mice compared with control mice (Figures 4E and 4F). These results suggested that overexpression of activin E in the liver stimulated the emergence of beige adipocytes in ingWAT and mesWAT. In fact, significant upregulation of Ucp1 expression was detected in ingWAT and mesWAT of Alb-ActE

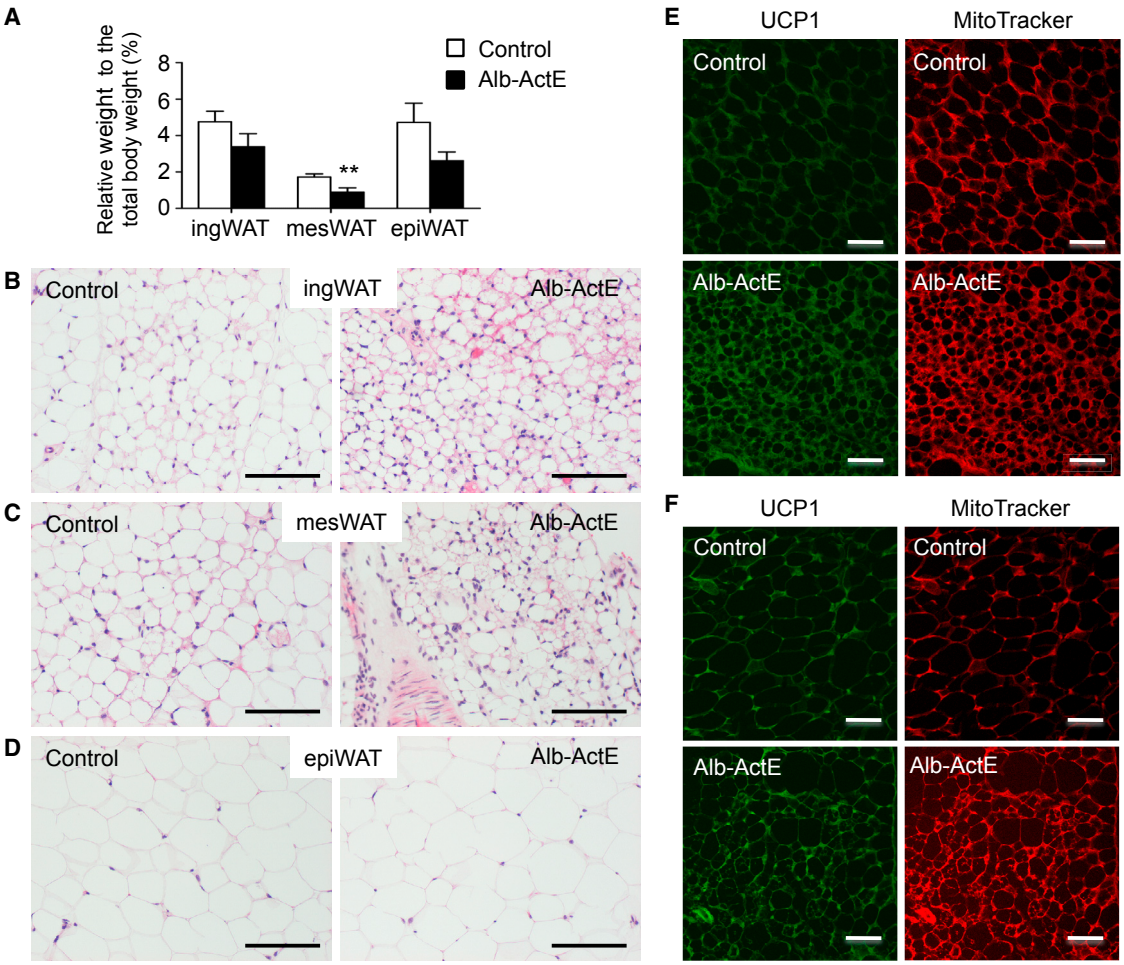

Figure 4. Characteristics of WAT in Alb-ActE Mice

(A) Adipose tissue weight in Alb-ActE mice. Relative tissue weight is expressed as a percentage of total body weight. Results are shown as means ± SEM. **$p < 0.01$. n = 4 in each group (18–24 weeks of age).

(B–D) H&E staining of WAT sections from the mice. (B) ingWAT, (C) mesWAT, (D) epiWAT. Representative data are shown. Bars, 100 μm.

(E and F) Fluorescence staining of UCP1 and mitochondria in ingWAT and mesWAT of Alb-ActE mice. WAT sections from mice (18 weeks of age) were reacted with MitoTracker and an anti-UCP1 antibody, and then incubated with a fluorescence-labeled second antibody. Fluorescent signals were observed using a fluorescence microscope. Representative data are shown. (E) ingWAT. (F) mesWAT. Bars, 50 μm. ing, inguinal; mes, mesenteric; epi, epididymal.

mice (Figure 5A). Unexpectedly, no significant differences were observed in expression of other genes with higher expression in brown and beige adipocytes than in white adipocytes (Seale et al., 2008; Wu et al., 2012), except for Prdm16 in mesWAT (Figures 5B–5I). Furthermore, *Fgf21* expression was upregulated in ingWAT and epiWAT of Alb-ActE mice (Figure 5J). In contrast, hepatic expression of *Fgf21* was decreased in Alb-ActE mice (Figure S5A). Serum Fgf21 concentrations were comparable in control and Alb-ActE mice (Figure S5B). We also measured the serum level of norepinephrine and expression level of *Adrb3* in adipose tissues to evaluate sympathetic nerve activity (Figure S5). Overexpression of hepatic activin E did not affect the serum norepinephrine level (Figure S5C) or expression level of *Adrb3* in ingWAT and mesWAT (Figure S5D). Furthermore, the expression level of *Adrb3* was higher in iBAT and lower in epiWAT.

Cold Intolerance through Less Emergence of Beige Adipocytes and Thermogenesis in Activin E-Knockout Mice

To determine the physiological role of activin E, we generated inhibin βE-ablated mice (Figures S6A–S6E). Targeted disruption of the inhibin βE gene did not affect the body weight, rectal temperature, plasma glucose, glucose and insulin tolerance, liver functions, or food intake of activin E-knockout (ActE-KO) mice at room temperature (22°C) (Figures S6F–S6M). In addition, the relative weights of iBAT, ingWAT, mesWAT, and epiWAT were comparable between wild-type and ActE-KO mice (Figure S7A). Histologically, there was no significant difference in their adipose tissues (Figure S7B). The expression level of *Ucp1* in ingWAT of wild-type mice was significantly lower than that in ingWAT of ActE-KO mice (Figure 6A). Unlike Alb-ActE mice, knockout of the *Inhbe* gene did not affect expression levels

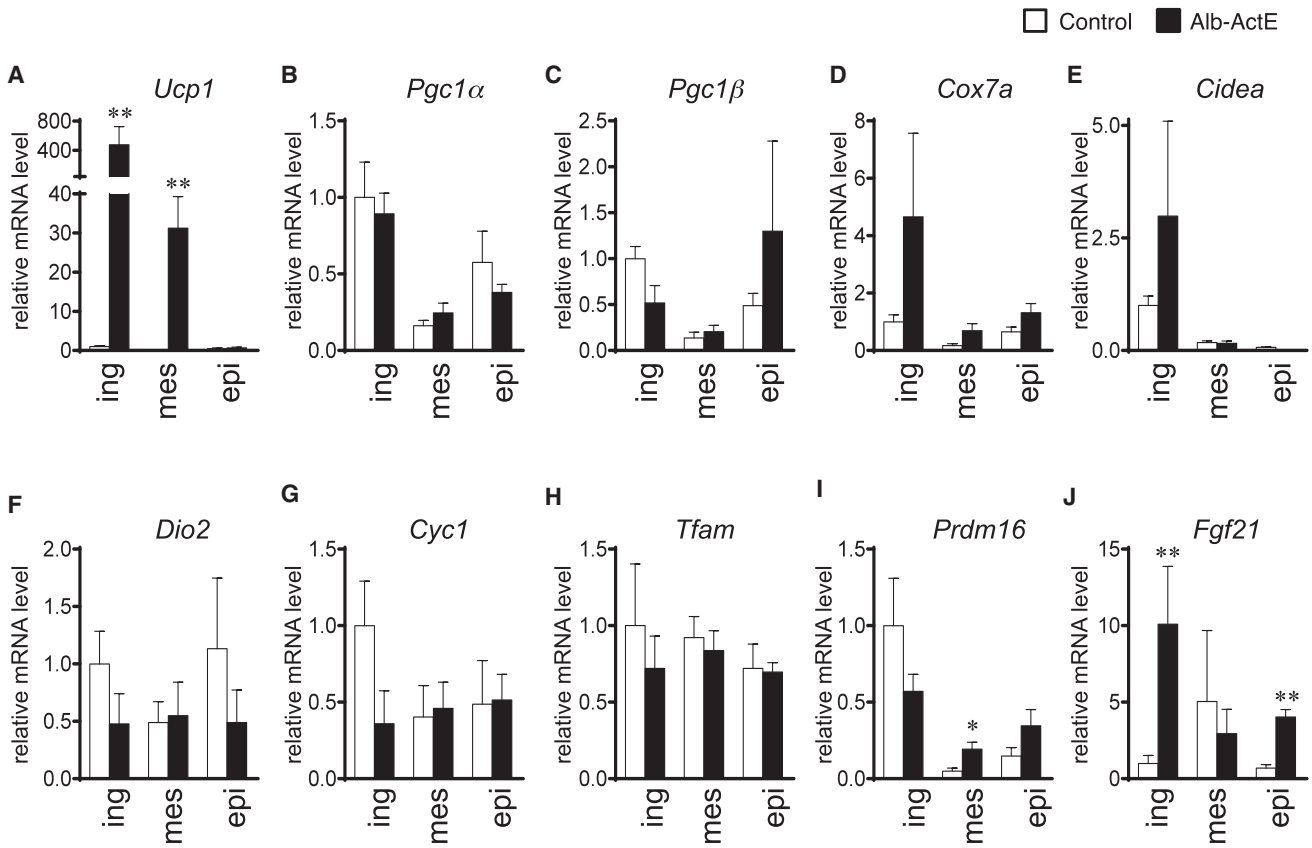

Figure 5. Expression of Brown Adipocyte-Specific Genes in WAT of Alb-ActE Mice

(A–J) mRNA from WAT of mice at 24–27 weeks of age was subjected to RT-qPCR. mRNA expression of *Ucp1* (A), *Pgc1α* (B), *Pgc1β* (C), *Cox7a* (D), *Cidea* (E), *Dio 2* (F), *Cyc1* (G), Tfam (H), *Prdm16* (I), *Fgf21* (J) in the WAT. Expression of the genes was normalized to that of Tbp. The expression level in control mice was set at 1. Data are shown as the mean ± SEM. *p < 0.05. n = 4 in each group. ing, inguinal; mes, mesenteric; epi, epididymal.

of *Fgf21* or *Bmp8b* in iBAT (Figure 6B). However, *Fgf21* expression was significantly lower in ingWAT of ActE-KO mice compared with that of wild-type mice (Figure 6C). Additionally, hepatic *Fgf21* expression tended to be higher in ActE-KO mice than in wild-type mice (Figure S7C), and serum Fgf21 levels were comparable in wild-type and ActE-KO mice (Figure S7D).

We next investigated adaptive thermogenesis during acute cold exposure in ActE-KO mice. Cold exposure at 4°C for 6 hr resulted in a significant reduction of rectal temperature in ActE-KO mice (Figure 6D). Emergence of beige adipocytes occurs within 6 hr after cold exposure (Dempersmier et al., 2015). We also observed rapid induction of beige adipocytes, and targeted disruption of the inhibin βE gene blocked the emergence of Ucp1-positive beige adipocytes induced by cold exposure (Figure 6E). These results suggest that activin E is required for induction of beige adipocytes and thermogenesis in response to cold exposure.

Activin E Directly Stimulates Differentiation of Brown Preadipocytes

We further explored the mechanism underlying modulation of the emergence of beige adipocytes related to the expression level of activin E. To this end, we performed *in vitro* experiments using iBPA cells, immortalized preadipocytes from mouse iBAT. During brown adipogenesis, cells were treated with or without conditioned medium (CM) from activin E-expressing cells (CM-ActE) or CM from cells transfected with the empty vector (CM-control). We attempted to prepare recombinant activin E protein using Chinese hamster ovary (CHO) cells. Unfortunately, during the purification step, activin E protein was lost by non-specific adsorption to the high-performance liquid chromatography column, and an insufficient amount of recombinant activin E was obtained. Expression levels of *Ucp1* and *Cidea* were increased at 10 hr after treatment with CM-ActE (Figures 7A and 7B). The CM-ActE also increased expression of *Fgf21* (Figure 7C). The upregulation of *Ucp1*, *Cidea*, and *Fgf21* expression was blocked by cotreatment with SB431542, an inhibitor of TGF-β or activin type I receptors (Callahan et al., 2002), but not with inhibitors of other signaling pathways (Figures 7D–7F).

DISCUSSION

Since functional brown and beige adipocytes were identified in adult humans, activation of brown and beige adipocytes has been suggested to be potentially helpful for prevention or

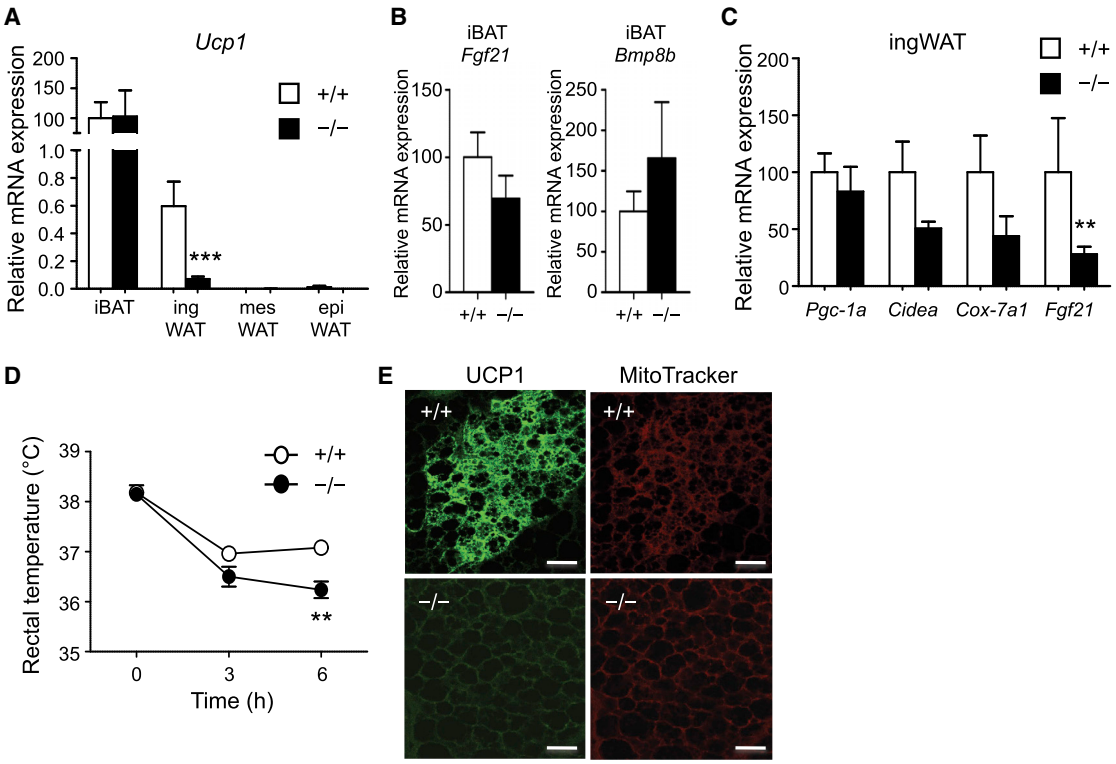

Figure 6. Impaired Thermogenesis through Less Emergence of Beige Adipocytes in ActE-KO Mice

(A) Ucp1 gene expression in adipose tissues of mice.

(B and C) Expression of *Fgf21* and *Bmp8b* in iBAT (B) and expression of brown adipocyte-selective genes in ingWAT (C) were examined by RT-qPCR. Expression of the genes was normalized to that of Tbp. The expression level in control mice was set at 1. Data are shown as the mean ± SEM. $^{**}p < 0.01$ and $^{***}p < 0.005$. Mice at 11–15 weeks of age were analyzed. n = 4 in each group. ing, inguinal; mes, mesenteric; epi, epididymal.

(D) Rectal temperature of ActE-KO mice exposed to 4°C. Mice at 14–34 weeks of age were analyzed. Data are shown as the mean ± SEM. $^{**}p < 0.01$. n = 5–11.

(E) Fluorescence staining of UCP1 and mitochondria in ingWAT from cold-challenged ActE-KO mice. ingWAT sections from mice (14 weeks of age) exposed to 4°C for 6 hr were reacted with MitoTracker and an anti-UCP1 antibody, and then incubated with a fluorescence-labeled second antibody. Fluorescent signals were observed using a fluorescence microscope. Representative data are shown. Bar, 50 μm.

therapeutic intervention of obesity (Stanford et al., 2013). The present study indicates that (1) activin E is required for cold-induced thermogenesis through induction of beige adipocytes in ingWAT, (2) overexpression of activin E enhances thermogenesis and insulin sensitivity through stimulation of brown adipocyte activity in iBAT as well as induction of beige adipocytes in ingWAT and mesWAT, (3) the expression level of activin E is closely related to that of Fgf21 in ingWAT, and (4) activin E enhances expression of *Ucp1* and *Fgf21* in cultured brown (pre)adipocytes. The present results uncovered a role of activin E as a hepatokine in regulation of energy metabolism through activation of brown and beige adipocytes.

Expression of *Ucp1* and *Fgf21* was increased in iBAT and ingWAT of activin E-transgenic mice, whereas their expression was decreased in ingWAT, but not iBAT, of ActE-KO mice. Owen et al. (2014) reported that FGF21 stimulates sympathetic nerve activity, leading to an increase in energy expenditure and weight loss in mice. In this study, plasma norepinephrine concentrations were not affected by the expression level of activin E. Furthermore, the serum FGF21 level was unaffected by the expression level of activin E resulting from the opposite effects of *Fgf21* expression in adipose tissues and the liver. Activin E-induced modulation of thermogenesis is unlikely to be mediated through activation of sympathetic nerve activity induced by increased production of FGF21. Nevertheless, in view of altered expression of *Adrb3* in iBAT and epiWAT of Alb-ActE mice, the activin E is likely to modulate signaling activity of norepinephrine depending on the fat depot.

Previous studies have shown that pharmacological FGF21 induces the emergence of Ucp1-positive adipocytes and increases beige adipocyte-related gene expression in ingWAT (Fisher et al., 2012). In addition, FGF21 increases expression levels of brown and beige adipocyte-selective genes including *Ucp1* in cultured brown and beige adipocytes (Fisher et al., 2012). Treatment with FGF21 during adipogenesis also stimulates *Ucp1* expression and oxygen consumption in human adipocytes (Lee et al., 2014). These results indicate direct effects of FGF21 in adipose tissues. Therefore, modulation of thermogenesis related to the activin E status is likely to be mediated through regulatory expression of adipose FGF21. In fact, activin E directly stimulated brown adipogenesis and expression of *Fgf21* in the *in vitro* experiments.

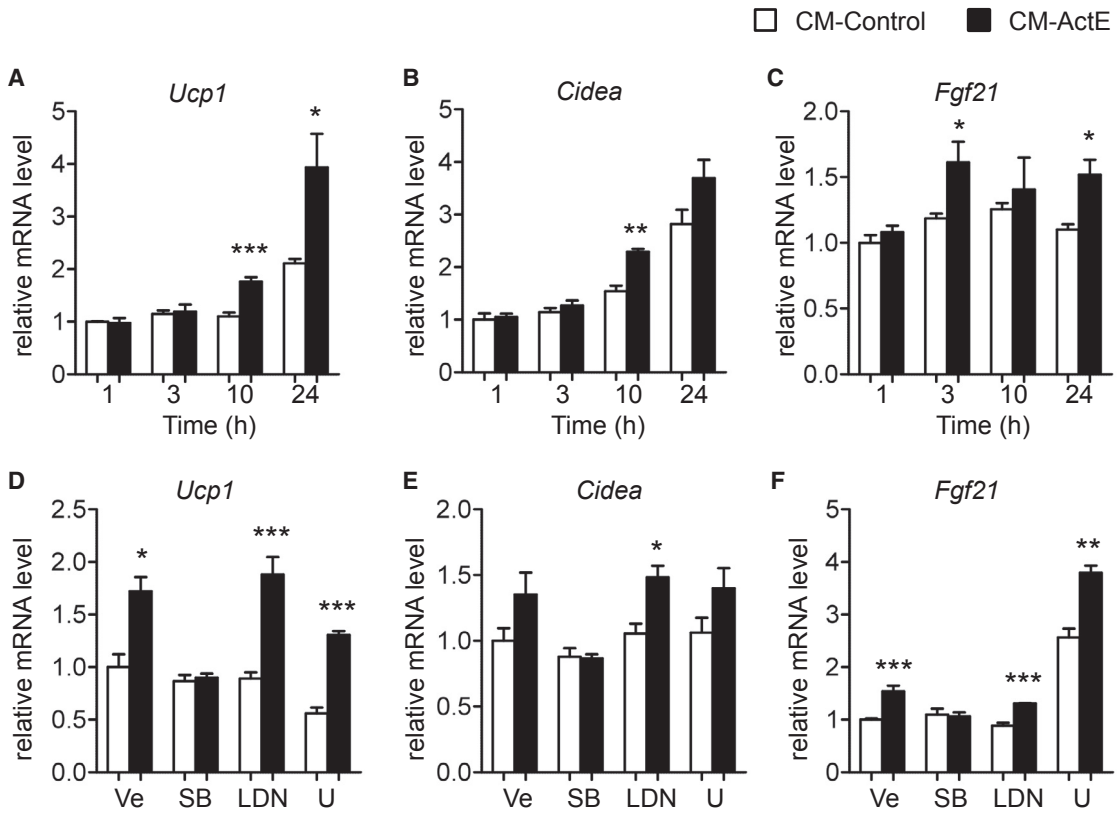

Figure 7. Activin E Regulates Expression of *Ucp1*, *Cidea*, and *Fgf21* via TGF-β or Activin Type I Receptors in Brown (Pre)adipocytes

(A–F) iBPA cells were induced to differentiate into brown adipocytes. Four days after the induction of differentiation, cells were treated with CM-ActE or CM-control for the indicated times (A–C) or for 24 hr in the presence of the indicated inhibitor (D–F). Expression levels of *Ucp1* (A and D), *Cidea* (B and E), and *Fgf21* (C and F) were examined by RT-qPCR. Expression of the genes was normalized to that of Gapdh. The expression level in cells treated with CM-control for 1 hr (A–C) or with CM-control in the presence of the vehicle (D–F) was set at 1. Data are shown as the mean ± SEM. *$p < 0.05$, **$p < 0.01$, and ***$p < 0.001$. $n = 3$ in each group. Ve, Vehicle; SB, SB431542; LDN, LDN193189; U, U0126.

Overexpression of activin E in Alb-ActE mice induced expression of Ucp1 in not only ingWAT but also other fat depots including iBAT and mesWAT, whereas the inability to induce Ucp1 expression was limited to ingWAT in ActE-KO mice. Although the reason why the affected fat depots were different between Alb-ActE and ActE-KO mice is unclear, the high blood flow rate in iBAT (Cannon and Nedergaard, 2004) likely enables an efficient response to the increase in the plasma activin E level of Alb-ActE mice. In addition, upregulation of *Ucp1* expression in iBAT of Alb-ActE mice may be related to increased expression of *Bmp8b*, because changes in the expression level of *Bmp8b* in iBAT paralleled those of Ucp1. A previous study has shown involvement of Bmp8b in activation of brown adipocytes (Whittle et al., 2012).

Our *in vitro* experiments indicated that activin E-induced *Ucp1* and *Fgf21* expression was suppressed by inhibition of TGF-β or activin type I receptors, i.e., Alk4, Alk5, and Alk7, but not Bmp type I receptors, i.e., Alk2, Alk3, and Alk6. Members of the TGF-β family signal via complex formation with specific receptors including type I and type II receptors (Budi et al., 2017). At present, receptors to confer activin E signals are unclear. Proteomic analysis has indicated that activin E forms a complex with Actr2b, an activin and Bmp type II receptor (Souza et al., 2008). Thus, it is possible that activin E signals via Alk4, Alk5, or Alk7 as a type I receptor and Actr2b as a type II receptor. Considering that Alk7 expression increases with progression of adipogenesis (Kogame et al., 2006), Alk7 may be a putative receptor for activin E.

The expression level of hepatic activin E is modulated in response to changes in the energy status. Inhibin βE mRNA increases by consuming a high-fat diet (Hashimoto et al., 2009). In addition, activin E expression is actively regulated within a day. The expression level of activin E increases gradually before a meal and rapidly decreases after refeeding of food-restricted rats exposed to time-scheduled feeding (Rodgarkia-Dara et al., 2006). Considering that beige adipocytes emerged rapidly in ingWAT in response to cold exposure (~6 hr), and that induction of the inguinal Ucp1 gene was less in ActE-KO mice, activin E may be involved in fine-tuning of thermogenesis induced by cold exposure. Considering the physiological role of activin E as shown by the gene-silenced mice and the pharmacological effect of activin E as shown by the transgenic mice, activin E may be a therapeutic target for obesity.

Recently, Sugiyama et al. (2018) reported that hepatic activin E may act as a putative candidate that alters whole-body energy metabolism under obese insulin-resistant conditions. Hepatic *INHBE* mRNA levels were positively correlated with insulin resistance in humans, and downregulation of *Inhbe* expression by injection of siRNA against *Inhbe* decreased fat mass through increased lipid utilization in db/db diabetic mice. These results suggest that activin E is a putative factor to induce insulin resistance, which contradicts the results shown in this study. At present, the reason for the inconsistent results is unknown, and future studies are needed to clarify the role of the hepatokine activin E.

EXPERIMENTAL PROCEDURES

Materials

The pCALNL5 vector (Kanegae et al., 1995), a Cre/loxP expression plasmid, was constructed by Dr. Izumu Saito (University of Tokyo) and provided by the RIKEN BioResource Center (Tsukuba, Japan). The anti-activin E antibody was prepared as described previously (Hashimoto et al., 2006). The anti-Ucp1 antibody was purchased from Abcam (Cambridge, UK; 2.5 μg/mL; catalog #ab10983, RRID:AB_2241462). Mice bearing the serum albumin gene promoter and enhancer-driven Cre recombinase (Alb-Cre) transgene (B6.Cg-Tg [Alb-cre]21Mgn/J) were purchased from The Jackson Laboratory (IMSR catalog #JAX:003574, RRID:IMSR_JAX:003574).

Generation of Transgenic Mice Overexpressing Hepatic Activin E and ActE-KO Mice

Transgenic mice carrying a flox-stopped mouse activin E transgene ($mActE^{flox}$) were generated using a Cre/loxP expression plasmid constructed with the pCALNL5 vector (Figure S2A) as described previously (McMahon et al., 2008). Mouse inhibin βE cDNA (mActE, NM_008382) was amplified by RT-PCR from mouse liver using primers 5′-TGCGAATTCACCTG GAGCATGAAACTTCCAAAAGCCCAG-3′ and 5′-TTAGGTACCCTAGCTGCA GCCACAGGCCTCTACTAC-3′, and inserted into the multi-cloning site of the vector. After confirmation of the mActE DNA sequence, the resulting vector was designated as pCALNL5-mActE.

The transgene was isolated by digestion with SalI and HindIII from pCALNL5-mActE, followed by agarose gel extraction. Microinjection of the linearized transgene into pronuclei of fertilized eggs from C57BL/6J mice performed by CLEA Japan (Transgenic Core; Tokyo, Japan) resulted in the production of mice that were determined to be transgenic by PCR genotyping using primers E1 (5′-TAGCCAAGCAGCAAATCCTGGA-3′) and E2 (5′-CTTT GAGGAGGCTGAAGACG-3′).

The founder mice (lines 2, 8, 25, and 28) were bred with C57BL/6J mice (CLEA Japan) to establish strains of $mActE^{flox}$-transgenic mice (C57BL/6J-Tg[CAG-floxed INHBE] Ohm).

Genotyping of each mouse revealed that four of these mice transmitted the transgene through the germline, as established by PCR genotyping. Lines 2, 8, and 25 of $mActE^{flox}$-transgenic mice did not reproduce well.

To examine the effect of activin E overexpression exclusively in the liver, female (line 28, IMSR catalog #RBRC04019, RRID:IMSR_RBRC04019) mice heterozygous for the $mActE^{flox}$ transgene were crossed with male mice homozygous for the Alb-Cre transgene to generate mice heterozygous for both mActE and Alb-Cre transgenes.

PCR analysis to detect both the floxed (2,055 bp) and recombined (1,105 bp) forms of the transgene in the liver was performed using primers C1 (5′-CTGC TAACCATGTTCATGCC-3′) and E2. Primers Cre-5 (5′-ACCTGAAGATGTTC GCGATTATCT-3′) and Cre-3 (5′-ACCGTCAGTACGTGAGATATCTT-3′) were used for PCR genotyping to detect Cre transgene (Postic et al., 1999).

Mice heterozygous for both $mActE^{flox}$ and Alb-Cre transgenes are referred to as transgenic mice (Alb-ActE mice). Mice heterozygous for the Alb-Cre transgene were used as experimental control mice (littermates).

For targeted disruption of the activin E gene, design of the target sequences and construction of the vectors for transcription activator-like effector nuclease (TALEN) were conducted by CELLECTIS Bioresearch (Romainville, France). TALENs were synthesized using methods similar to those described elsewhere (Cermak et al., 2011). The DNA binding sites for the TALEN pair targeting *Inhbe* (NM_008382) were 5′-TGCAGAGTACAAGATCT-3′ and 5′-TGC CAGTGTTGGGCCCC-3′ (Figure S6A). The RNA fragments for TALENs were generated using the T7 promoter and microinjected into pronuclei of fertilized eggs from C57BL/6J mice. The zygotes were transferred into oviducts of pseudo-pregnant ICR female mice, and founder mice were derived. To detect mutant mice, genomic DNA was isolated from tail biopsies and analyzed by PCR amplification using a primer set (5′-TCGAGGTTCTCAAAGCAGAG-3′ and 5′-GATGACTTTCTCTCGGTTGC-3′). The deletion of *Inhbe* was subsequently confirmed by DNA sequencing of PCR products. Only 1 of the 135 mice was determined to have the mutation in exon I of the *Inhbe* gene. The mutation was a 46-bp deletion that gave rise to a frameshift. Therefore, a truncated protein would be produced (Figures S6B and S6C). This female founder mouse was bred with wild-type C57BL/6J male mice to generate the mutant strain.

RT-PCR analysis of *Inhbe* mRNA from the mutant liver was performed using a primer set (5′-TGCGAATTCACCTGGAGCATGAAACTTCCAAAAGCC CAG-3′ and 5′-TTAGGTACCCTAGCTGCAGCCACAGGCCTCTACTAC-3′). The products were inserted into the multi-cloning site of the expression vector and confirmed by sequencing (Figure S6D).

Male mice were used for all experiments. Mice housed individually from 6 weeks of age were maintained in a 12-hr light/dark cycle at 22 ± 4°C and provided standard chow (CE-2; CLEA Japan) and water *ad libitum*. Experimental procedures and the care of animals were performed in accordance with the requirements of the Institutional Animal Care Committee at Kitasato University and in compliance with National Institutes of Health guidelines (17-008).

Determination of Circulating Activin E, Fgf21, and Norepinephrine Levels

Serum concentrations of activin E and Fgf21 were measured by an inhibin βE ELISA kit (CEA048Mu; Cloud-Clone Corporation, Katy, TX, USA) and Fgf-21 ELISA kit (MF2100; R&D Systems, Minneapolis, MN, USA), respectively. Plasma levels of norepinephrine were measured by an ELISA kit (KA 1877; Abnova, Taipei, Taiwan).

Physiological Measurements

Mice were weighed weekly from 4 to 52 weeks of age. Food intake of the mice was measured for 2–4 days, and average intake per day was calculated. Rectal temperature was monitored in mice using a microprobe thermometer system equipped with a rectal probe (model BAT-12; Muromachi Kikai Company, Tokyo, Japan) at 15:00–17:00 hr during the light cycle. Respiratory gas analysis was performed with an Arco-2000 (Arco System, Chiba, Japan) as described previously (Ishihara et al., 2000). Oxidation of lipid and carbohydrate were computed based on oxygen consumption (VO_2) and carbon dioxide production (VCO_2). VO_2 and VCO_2 data were presented as milliliters per minute per kilogram of total body weight. Behavior of the mice in their home cage was recorded on video. The duration of locomotion of Alb-ActE mice was measured for 24 hr.

Histological Analysis

Tissues from mice were weighed, fixed in Bouin's fluid, and embedded in paraffin. Sections of 4 μm in thickness were affixed to slides. Cell sizes were examined using H&E-stained adipose tissues. Four arbitrary fields of view (0.12 mm^2/WAT per field) were analyzed by ImageJ 1.62 (NIH) to estimate the adipocyte area. Subsequently, the density and distribution of adipocytes were calculated.

For immunohistochemistry, a rabbit polyclonal anti-Ucp1 antibody (3 μg/mL; ab10983; Abcam) was reacted with deparaffinized sections overnight at 4°C and visualized with 3,3′-diaminobenzidine tetrahydrochloride using a Histofine Simple Stain MAX-PO kit (Nichirei, Tokyo, Japan) as described previously (Hashimoto et al., 2006).

For fluorescence staining, deparaffinized sections were blocked with 1% normal goat serum for 5 hr at 4°C and then reacted with MitoTracker Red CMXRos (1:25,000; Thermo Fisher Scientific, Waltham, MA, USA) and a rabbit anti-UCP1 antibody (1:1,000; UCP11-A; Alpha Diagnostic International, San

Antonio, TX, USA) overnight at 4°C. The sections were washed three times with PBS and incubated with Alexa Fluor 488 goat anti-rabbit IgG (Thermo Fisher Scientific). Fluorescent signals were observed using a BZ-9000 fluorescence microscope (Keyence, Osaka, Japan).

Blood Examination

For the glucose tolerance test, glucose (1 mg per 1 g body weight) was administrated intraperitoneally to anesthetized mice after 16 hr of fasting. For the insulin tolerance test, mice were anesthetized and 2 mU of insulin (Novolin 30R; Novo Nordisk, Denmark) per 1 g of body weight was intraperitoneally administrated after 4 hr of fasting. Blood was drawn from the caudal vein at the indicated times. The blood glucose level was measured by a Medisafe (Terumo, Tokyo, Japan). The plasma insulin level was measured by an immunoassay kit (Mouse Insulin ELISA kit U-type; Shibayagi, Gunma, Japan).

Intravenous blood was obtained via the caudal vena cava from 4-hr-fasted mice under anesthesia induced by pentobarbital. Serum was then isolated and assayed for blood parameters of liver functions using kits (Wako Pure Chemical Industries, Osaka, Japan).

RNA Isolation and Real-Time RT-qPCR

Total RNA was isolated from iBAT, ingWAT, mesWAT, and epiWAT using an RNeasy Lipid Tissue Mini Kit (Qiagen, Hilden, Germany). cDNA was prepared using a ReverTra Ace qPCR RT Kit (Toyobo, Osaka, Japan); cDNA reverse transcribed from 5 ng of total RNA was used as a template for real-time qPCR using Thunderbird SYBR qPCR Mix (Toyobo) as described previously (Kida et al., 2016). The oligonucleotide primers for RT-qPCR are presented in Table S1. The Ct value was determined, and the abundance of gene transcripts was analyzed by the ΔΔCt method using TATA-binding protein (Tbp) as the normalization gene.

Western Blotting

Tissues were rinsed in ice-cold PBS and homogenized in RIPA lysis buffer (50 mM Tris-HCl, pH 7.4, 0.15 M NaCl, 0.25% deoxycholic acid, 1% NP-40, and 1 mM EDTA) containing a protease inhibitor cocktail. The proteins were subjected to SDS-polyacrylamide gel electrophoresis on 12% gels under reducing or non-reducing conditions and then transferred onto a polyvinylidene difluoride membrane (Millipore, Billerica, MA, USA). The membranes were blocked with 5% dry non-fat milk and probed with anti-hActE (Hashimoto et al., 2006), anti-Ucp1 (Alpha Diagnostic), or anti-β-actin (Abcam) antibodies, followed by incubation with a horseradish peroxidase-conjugated secondary antibody. The reaction was detected with a chemiluminescence system (ECL Plus; Amersham Biosciences). The band intensity was measured by ImageJ 1.37.

Preparation of CM

Human embryonic kidney 293 cells (RIKEN Cell Bank, Tsukuba, Japan) were maintained in DMEM/F12 (Invitrogen, Carlsbad, CA, USA) supplemented with 10% heat-inactivated fetal bovine serum, 100 U/mL penicillin, and 100 μg/mL streptomycin. The cells were seeded in 10-cm dishes at a density of 7.5×10^6 cells/dish and transfected with a human activin E expression vector (Hashimoto et al., 2006) or the empty vector using FuGene6 transfection reagent (Roche Diagnostics, Indianapolis, IN, USA), according to the manufacturer's instructions. At 24 hr after transfection, the cells were washed with 10 mL of PBS three times and incubated with DMEM/F12 containing 0.1% bovine serum albumin (5 mL/dish) for 4 days. The culture supernatants from cells transfected with human activin E or empty vectors were collected as CM-ActE and CM-control, respectively.

Cell Culture

iBPA cells are stromal vascular cells from neonatal C57BL/6J mouse iBAT immortalized by infection of the retroviral vector pBabe encoding the SV40 T antigen (Klein et al., 2002). The cells were maintained in DMEM (Sigma, St. Louis, MO, USA) supplemented with 10% heat-inactivated fetal bovine serum, 100 U/mL penicillin, and 100 μg/mL streptomycin (growth medium). They were seeded in 24-well plates at a density of 2×10^5 cells per well. At 24 hr after seeding (day 0), the cells were treated with growth medium containing 10 nM insulin, 1 nM T_3, 0.5 mM IBMX, 0.5 μM dexamethasone, and 0.125 mM indomethacin for 48 hr. The cells were subsequently cultured in growth medium containing 10 nM insulin and 1 nM T_3. The medium was changed every 2 days. On day 4, the cells were treated with CM-ActE or CM-control (100 μL/500 μL growth medium/well) for the indicated times in the absence or presence of inhibitors (SB431542 [10 μM], LDN193189, an inhibitor of BMP type I receptor [Cuny et al., 2008] [100 nM], and U0126, an inhibitor of MEK1/2 [Favata et al., 1998] [10 μM]).

Statistical Analyses

Results are expressed as means ± SEM. Gene expression data were log-transformed to provide an approximation of a normal distribution before analyses. Student's t tests were performed to compare two sets of data. The Dunnett multiple-comparison test was used to compare results among groups. Statistical analyses were conducted using Prism5 software (GraphPad Software, San Diego, CA, USA). A value of $p < 0.05$ was considered as statistically significant.

SUPPLEMENTAL INFORMATION

Supplemental Information includes seven figures and one table and can be found with this article online at https://doi.org/10.1016/j.celrep.2018.10.008.

ACKNOWLEDGMENTS

We thank Dr. Nicholas Webster for critical reading, Drs. Nobuyuki Itoh and Shingo Kajimura for discussions, and Dr. Izumi Saito for the pCALNL5 vector. O.H. was supported by a Grant-in-Aid for Scientific Research from The Japan Society for the Promotion of Science (JSPS KAKENHI Grant JP21580370). M.F. was supported by JSPS KAKENHI Grant JP26450442. A.K. was supported by JSPS KAKENHI Grant JP25640109. We thank Mitchell Arico from Edanz Group (https://www.edanzediting.com/ac) for editing a draft of this manuscript.

AUTHOR CONTRIBUTIONS

The study was designed by O.H., M.F., H.S., and A.K. Experimental analysis was performed by O.H., M.F., K.S., S.D., D.S., R.S., H.I., H.O., M.M. C.S., M.S., N.Y., H.T., and S.O. Metabolic cage experiments were performed by S.M., K.I., and S.O. The manuscript was written by O.H., M.F., and A.K.

DECLARATION OF INTERESTS

The authors declare no competing interests.

Received: January 23, 2018
Revised: June 12, 2018
Accepted: September 28, 2018
Published: October 30, 2018

REFERENCES

Budi, E.H., Duan, D., and Derynck, R. (2017). Transforming growth factor-β receptors and Smads: regulatory complexity and functional versatility. Trends Cell Biol. *27*, 658–672.

Callahan, J.F., Burgess, J.L., Fornwald, J.A., Gaster, L.M., Harling, J.D., Harrington, F.P., Heer, J., Kwon, C., Lehr, R., Mathur, A., et al. (2002). Identification of novel inhibitors of the transforming growth factor β1 (TGF-β1) type 1 receptor (ALK5). J. Med. Chem. *45*, 999–1001.

Cannon, B., and Nedergaard, J. (2004). Brown adipose tissue: function and physiological significance. Physiol. Rev. *84*, 277–359.

Cereijo, R., Villarroya, J., and Villarroya, F. (2015). Non-sympathetic control of brown adipose tissue. Int. J. Obes. Suppl. *5* (*Suppl 1*), S40–S44.

Cermak, T., Doyle, E.L., Christian, M., Wang, L., Zhang, Y., Schmidt, C., Baller, J.A., Somia, N.V., Bogdanove, A.J., and Voytas, D.F. (2011). Efficient design and assembly of custom TALEN and other TAL effector-based constructs for DNA targeting. Nucleic Acids Res. *39*, e82.

Chabicovsky, M., Herkner, K., and Rossmanith, W. (2003). Overexpression of activin β(C) or activin β(E) in the mouse liver inhibits regenerative deoxyribonucleic acid synthesis of hepatic cells. Endocrinology *144*, 3497–3504.

Cousin, B., Cinti, S., Morroni, M., Raimbault, S., Ricquier, D., Pénicaud, L., and Casteilla, L. (1992). Occurrence of brown adipocytes in rat white adipose tissue: molecular and morphological characterization. J. Cell Sci. *103*, 931–942.

Cuny, G.D., Yu, P.B., Laha, J.K., Xing, X., Liu, J.F., Lai, C.S., Deng, D.Y., Sachidanandan, C., Bloch, K.D., and Peterson, R.T. (2008). Structure-activity relationship study of bone morphogenetic protein (BMP) signaling inhibitors. Bioorg. Med. Chem. Lett. *18*, 4388–4392.

Dempersmier, J., Sambeat, A., Gulyaeva, O., Paul, S.M., Hudak, C.S., Raposo, H.F., Kwan, H.Y., Kang, C., Wong, R.H., and Sul, H.S. (2015). Cold-inducible Zfp516 activates UCP1 transcription to promote browning of white fat and development of brown fat. Mol. Cell *57*, 235–246.

Fang, J., Wang, S.Q., Smiley, E., and Bonadio, J. (1997). Genes coding for mouse activin β C and β E are closely linked and exhibit a liver-specific expression pattern in adult tissues. Biochem. Biophys. Res. Commun. *231*, 655–661.

Favata, M.F., Horiuchi, K.Y., Manos, E.J., Daulerio, A.J., Stradley, D.A., Feeser, W.S., Van Dyk, D.E., Pitts, W.J., Earl, R.A., Hobbs, F., et al. (1998). Identification of a novel inhibitor of mitogen-activated protein kinase kinase. J. Biol. Chem. *273*, 18623–18632.

Fisher, F.M., Kleiner, S., Douris, N., Fox, E.C., Mepani, R.J., Verdeguer, F., Wu, J., Kharitonenkov, A., Flier, J.S., Maratos-Flier, E., and Spiegelman, B.M. (2012). FGF21 regulates PGC-1α and browning of white adipose tissues in adaptive thermogenesis. Genes Dev. *26*, 271–281.

Harms, M., and Seale, P. (2013). Brown and beige fat: development, function and therapeutic potential. Nat. Med. *19*, 1252–1263.

Hashimoto, O., Tsuchida, K., Ushiro, Y., Hosoi, Y., Hoshi, N., Sugino, H., and Hasegawa, Y. (2002). cDNA cloning and expression of human activin betaE subunit. Mol. Cell. Endocrinol. *194*, 117–122.

Hashimoto, O., Ushiro, Y., Sekiyama, K., Yamaguchi, O., Yoshioka, K., Mutoh, K., and Hasegawa, Y. (2006). Impaired growth of pancreatic exocrine cells in transgenic mice expressing human activin betaE subunit. Biochem. Biophys. Res. Commun. *341*, 416–424.

Hashimoto, O., Sekiyama, K., Matsuo, T., and Hasegawa, Y. (2009). Implication of activin E in glucose metabolism: transcriptional regulation of the inhibin/activin betaE subunit gene in the liver. Life Sci. *85*, 534–540.

Ishihara, K., Oyaizu, S., Onuki, K., Lim, K., and Fushiki, T. (2000). Chronic (−)-hydroxycitrate administration spares carbohydrate utilization and promotes lipid oxidation during exercise in mice. J. Nutr. *130*, 2990–2995.

Kanegae, Y., Lee, G., Sato, Y., Tanaka, M., Nakai, M., Sakaki, T., Sugano, S., and Saito, I. (1995). Efficient gene activation in mammalian cells by using recombinant adenovirus expressing site-specific Cre recombinase. Nucleic Acids Res. *23*, 3816–3821.

Kida, R., Yoshida, H., Murakami, M., Shirai, M., Hashimoto, O., Kawada, T., Matsui, T., and Funaba, M. (2016). Direct action of capsaicin in brown adipogenesis and activation of brown adipocytes. Cell Biochem. Funct. *34*, 34–41.

Klein, J., Fasshauer, M., Klein, H.H., Benito, M., and Kahn, C.R. (2002). Novel adipocyte lines from brown fat: a model system for the study of differentiation, energy metabolism, and insulin action. BioEssays *24*, 382–388.

Kogame, M., Matsuo, S., Nakatani, M., Kurisaki, A., Nishitani, H., Tsuchida, K., and Sugino, H. (2006). ALK7 is a novel marker for adipocyte differentiation. J. Med. Invest. *53*, 238–245.

Lau, A.L., Kumar, T.R., Nishimori, K., Bonadio, J., and Matzuk, M.M. (2000). Activin betaC and betaE genes are not essential for mouse liver growth, differentiation, and regeneration. Mol. Cell. Biol. *20*, 6127–6137.

Lee, P., Werner, C.D., Kebebew, E., and Celi, F.S. (2014). Functional thermogenic beige adipogenesis is inducible in human neck fat. Int. J. Obes. *38*, 170–176.

Lepper, C., and Fan, C.M. (2010). Inducible lineage tracing of Pax7-descendant cells reveals embryonic origin of adult satellite cells. Genesis *48*, 424–436.

McMahon, H.E., Hashimoto, O., Mellon, P.L., and Shimasaki, S. (2008). Oocyte-specific overexpression of mouse bone morphogenetic protein-15 leads to accelerated folliculogenesis and an early onset of acyclicity in transgenic mice. Endocrinology *149*, 2807–2815.

Owen, B.M., Ding, X., Morgan, D.A., Coate, K.C., Bookout, A.L., Rahmouni, K., Kliewer, S.A., and Mangelsdorf, D.J. (2014). FGF21 acts centrally to induce sympathetic nerve activity, energy expenditure, and weight loss. Cell Metab. *20*, 670–677.

Postic, C., Shiota, M., Niswender, K.D., Jetton, T.L., Chen, Y., Moates, J.M., Shelton, K.D., Lindner, J., Cherrington, A.D., and Magnuson, M.A. (1999). Dual roles for glucokinase in glucose homeostasis as determined by liver and pancreatic β cell-specific gene knock-outs using Cre recombinase. J. Biol. Chem. *274*, 305–315.

Rodgarkia-Dara, C., Vejda, S., Erlach, N., Losert, A., Bursch, W., Berger, W., Schulte-Hermann, R., and Grusch, M. (2006). The activin axis in liver biology and disease. Mutat. Res. *613*, 123–137.

Seale, P., Bjork, B., Yang, W., Kajimura, S., Chin, S., Kuang, S., Scimè, A., Devarakonda, S., Conroe, H.M., Erdjument-Bromage, H., et al. (2008). PRDM16 controls a brown fat/skeletal muscle switch. Nature *454*, 961–967.

Souza, T.A., Chen, X., Guo, Y., Sava, P., Zhang, J., Hill, J.J., Yaworsky, P.J., and Qiu, Y. (2008). Proteomic identification and functional validation of activins and bone morphogenetic protein 11 as candidate novel muscle mass regulators. Mol. Endocrinol. *22*, 2689–2702.

Stanford, K.I., Middelbeek, R.J.W., Townsend, K.L., An, D., Nygaard, E.B., Hitchcox, K.M., Markan, K.R., Nakano, K., Hirshman, M.F., Tseng, Y.H., and Goodyear, L.J. (2013). Brown adipose tissue regulates glucose homeostasis and insulin sensitivity. J. Clin. Invest. *123*, 215–223.

Sugiyama, M., Kikuchi, A., Misu, H., Igawa, H., Ashihara, M., Kushima, Y., Honda, K., Suzuki, Y., Kawabe, Y., Kaneko, S., and Takamura, T. (2018). Inhibin βE (INHBE) is a possible insulin resistance-associated hepatokine identified by comprehensive gene expression analysis in human liver biopsy samples. PLoS One *13*, e0194798.

Tschöp, M.H., Speakman, J.R., Arch, J.R., Auwerx, J., Brüning, J.C., Chan, L., Eckel, R.H., Farese, R.V., Jr., Galgani, J.E., Hambly, C., et al. (2011). A guide to analysis of mouse energy metabolism. Nat. Methods *9*, 57–63.

Vejda, S., Erlach, N., Peter, B., Drucker, C., Rossmanith, W., Pohl, J., Schulte-Hermann, R., and Grusch, M. (2003). Expression of activins C and E induces apoptosis in human and rat hepatoma cells. Carcinogenesis *24*, 1801–1809.

Vitali, A., Murano, I., Zingaretti, M.C., Frontini, A., Ricquier, D., and Cinti, S. (2012). The adipose organ of obesity-prone C57BL/6J mice is composed of mixed white and brown adipocytes. J. Lipid Res. *53*, 619–629.

Wada, W., Medina, J.J., Kuwano, H., and Kojima, I. (2005). Comparison of the function of the β(C) and β(E) subunits of activin in AML12 hepatocytes. Endocr. J. *52*, 169–175.

Whittle, A.J., Carobbio, S., Martins, L., Slawik, M., Hondares, E., Vázquez, M.J., Morgan, D., Csikasz, R.I., Gallego, R., Rodriguez-Cuenca, S., et al. (2012). BMP8B increases brown adipose tissue thermogenesis through both central and peripheral actions. Cell *149*, 871–885.

Wu, J., Boström, P., Sparks, L.M., Ye, L., Choi, J.H., Giang, A.H., Khandekar, M., Virtanen, K.A., Nuutila, P., Schaart, G., et al. (2012). Beige adipocytes are a distinct type of thermogenic fat cell in mouse and human. Cell *150*, 366–376.

Yen, M., and Ewald, M.B. (2012). Toxicity of weight loss agents. J. Med. Toxicol. *8*, 145–152.